

Noise and coupling in magnetic super-resolution media for magneto-optical readout

Cite as: Journal of Applied Physics **85**, 6323 (1999); <https://doi.org/10.1063/1.370133>

Submitted: 01 October 1998 . Accepted: 26 January 1999 . Published Online: 22 April 1999

Chubing Peng, and M. Mansuripur



View Online



Export Citation

Ultra High Performance SDD Detectors



See all our XRF Solutions

Noise and coupling in magnetic super-resolution media for magneto-optical readout

Chubing Peng^{a)} and M. Mansuripur

Optical Sciences Center, The University of Arizona, Tucson, Arizona 85721

(Received 1 October 1998; accepted for publication 26 January 1999)

Interfacial magnetic coupling, transient thermal response, and carrier and noise levels are investigated for two central aperture detection magnetic super-resolution disks. In one of the disks, the two magnetic layers are exchange-coupled, while in the other the coupling is of magneto-static nature. For the exchange-coupled disk, the coupling between the two magnetic layers is fairly strong, and the Kerr loop of the readout layer does not have a square shape. For the magneto-statically coupled disk, the strength of coupling depends on the nonuniformity of the magnetization of the storage layer. The readout layer has a square Kerr loop, but its perpendicular magnetization in the hot region under the focused spot has random orientation if the stray field from the storage layer is weak. This random orientation of magnetization within the readout layer gives rise to a high level of noise during readout. © 1999 American Institute of Physics.

[S0021-8979(99)04209-7]

I. INTRODUCTION

In magneto-optical (MO) data storage, magnetically-induced super resolution (MSR) is one of the promising technologies for realizing high-density recording. Using MSR, sub-micron magnetic domains can be detected with adequate carrier to noise ratio (CNR) by thermally forming an effective aperture which is smaller than the diffraction-limited size of the focused optical spot. Various MSR schemes have been proposed;¹⁻¹¹ among them, central aperture detection (CAD) requires no initialization or bias field for readout. The CAD-MSR disk usually consists of two or three magnetic layers. The magnetization of the readout layer (RL) is in-plane at room temperature but becomes perpendicular at the high temperatures reached during readout. Domains beneath the heated area can be detected while those in the adjacent areas are masked. In the three-layer structure, an intermediate layer is used to mediate the coupling between the RL and the storage layer (SL), tailoring the magnetic coupling between RL and SL and causing an abrupt transition of the RL polar Kerr signal with the rise in temperature. The intermediate layer between RL and SL can be a dielectric layer^{3,9} or a magnetic layer.⁶

In CAD-MSR disks, the RL is usually an amorphous film of GdFeCo alloy. At room temperature, the in-plane magnetization of this film has random orientation. In the heated area underneath the focused spot, because of the lateral exchange coupling to the adjacent in-plane moments, the perpendicular magnetization may acquire a degree of randomness, which will manifest itself as noise in readout. In this article, we present experimental data on magnetic coupling and noise characteristics for exchange-coupled and magneto-statically coupled CAD-MSR disks.

II. EXPERIMENTS

A static tester is used for evaluating the transient thermal response of the Kerr signal and investigating the magnetic coupling between RL and SL. Figure 1 is a schematic diagram of the static tester. It consists of a conventional white-light polarizing microscope augmented with a 780 nm laser diode and a differential detection module. The collimated laser beam from the laser diode is directed into the forward optical path of the microscope by a dichroic mirror and focused by the objective lens onto the sample. The reflected beam from the sample is then directed to the detection module, which generates the total (sum) signal, as well as the differential MO signal (ΔS). From these signals the polar Kerr rotation angle (θ_k) can be derived. During experiments, a magnetic field (H) perpendicular to the plane of the sample can be applied. In the following static measurements the objective lens used for focus has a numerical aperture of 0.6.

A dynamic tester is used for measurements of signal and noise spectra.¹² It uses a laser diode operating at 690 nm wavelength and a 0.6 NA objective lens. Light intensity modulation is used for writing, while readout is performed with a continuous beam. The magnitude of carrier and noise are evaluated using a spectrum analyzer with a bandwidth of 30 kHz. In the dynamic tester, the leaky polarizing beam splitter is set to have an amplitude leak ratio of 0.35 during readout.

Two CAD-MSR samples used for experiments are shown schematically in Fig. 2. Sample 1 consists of SiN/GdFeCo/TbFeCo/SiN/Al alloy/polycarbonate substrate. The polycarbonate substrate is grooved with track pitch of 1.1 μm . Sample 2 consists of glass substrate/SiN/GdFeCo/SiN/TbFeCo/SiN/Al alloy. The glass substrate, also grooved, has a track pitch of 1.6 μm . In both samples, the GdFeCo readout layer, about 40 nm thick, has compensation temperature well above room temperature ($\sim 260^\circ\text{C}$), whereas the

^{a)}Electronic mail: cpeng@u.arizona.edu

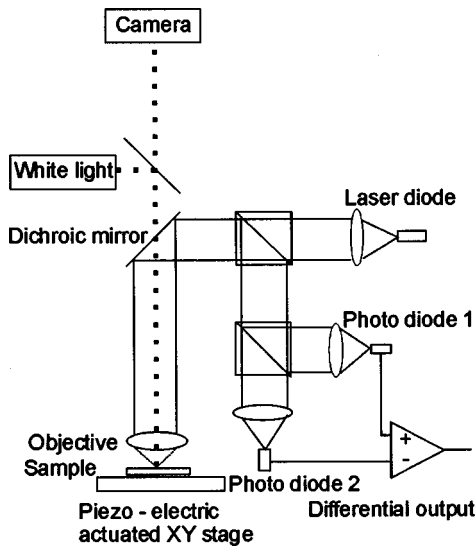


FIG. 1. Schematic diagram showing the static tester. The laser beam is focused on the sample, which rests on a piezo-electric XY stage. The reflected beam is detected by two photodiodes, yielding the differential magneto-optical signal. The piezo-actuated XY stage is used for scanning a small area of the sample.

TbFeCo storage layer has compensation temperature close to room temperature. In both samples, the GdFeCo alloy is confirmed to have in-plane magnetization at room temperature. In sample 2, the thickness of the SiN between the GdFeCo and TbFeCo is about 10 nm. In the static and dynamic measurements, the light beam is focused onto the film from surface side for sample 1 and through the substrate for sample 2; the objective lens is correspondingly corrected for film incidence or for substrate incidence. From the multilayer structure of the two samples shown in Fig. 2, it is evident that in sample 1 the RL and SL are mainly exchange-coupled, whereas in sample 2 the coupling is of magneto-static nature.

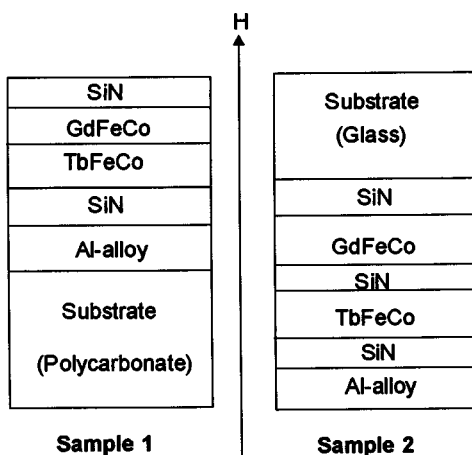


FIG. 2. Schematic diagram showing the structure of the two disks and the positive direction of the external magnetic field. In both samples, the GdFeCo layer is the readout layer and the TbFeCo layer is the storage layer.

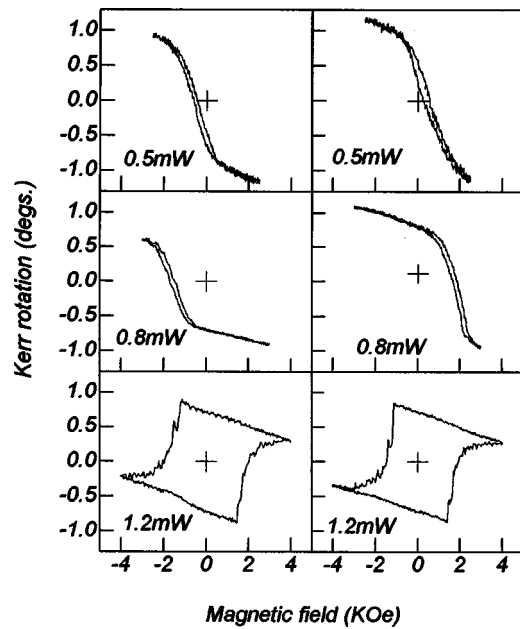


FIG. 3. Kerr hysteresis loops for sample 1, obtained under a focused laser beam at the reading powers of 0.5, 0.8, and 1.2 mW. The loops in the left column were obtained when the SL magnetization was saturated in a large negative magnetic field, $H < 0$. The loops in the right column were obtained after saturation in the reverse direction, $H > 0$.

III. RESULTS AND DISCUSSIONS

A. Kerr hysteresis loop

Since the temperature distribution under the focused spot is not uniform, one may expect that the Kerr loop trace obtained with the static tester will be complicated. However, measurements on a conventional MO disk have shown that the magnetic alloy exhibits a square Kerr loop. This feature of the Kerr hysteresis loop under a focused spot is probably due to the strong exchange coupling between magnetic moments in the MO layer, which causes all magnetic moments under the hot spot to reverse at the same magnetic field. Figures 3 and 4 show the RL Kerr loop traces for samples 1 and 2, obtained at various laser powers. Prior to tracing the loops, the SL was saturated at $H < 0$ (left column in Figs. 3 and 4) or $H > 0$ (right column). The magnetic coupling between RL and SL manifests itself as a bias field (H_b) which displaces the hysteresis curves relative to the vertical axis.

For sample 1, the Kerr loops in Fig. 3 show hysteresis, but they are not square. At the read powers of $P_0 = 0.5$ and 0.8 mW, θ_k increases with the increasing magnetic field after magnetization reversal. The exchange coupling through the magnetic moments of transition metals at the interface between RL and SL gives rise to $H_b < 0$ in the left column, but $H_b > 0$ in the right column.

From Fig. 3, H_b is seen to increase rapidly with the read power. At $P_0 = 1.2$ mW, the RL loops are inverted from those at $P_0 = 0.5$ and 0.8 mW, and θ_k decreases with increasing magnetic field after magnetization reversal. At this read power, the exchange coupling between RL and SL is larger than the SL coercivity, and, therefore, no RL Kerr loop trace can be obtained without reversing the SL magnetization. The reversal of RL magnetization in the external field follows

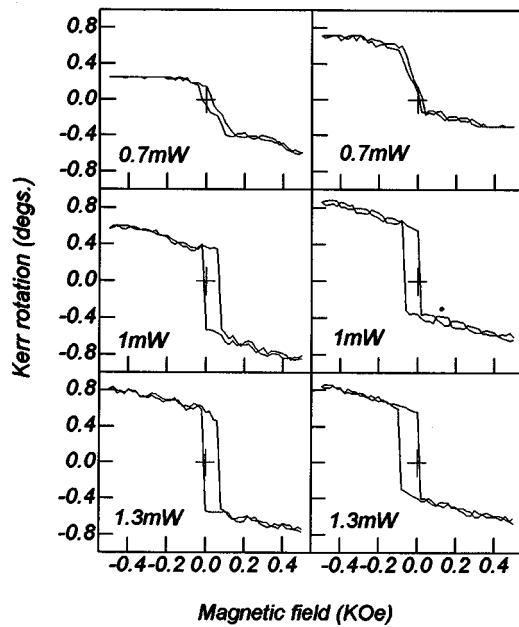


FIG. 4. Kerr hysteresis loops for sample 2, obtained under a focused laser beam at the reading powers of 0.7, 1, and 1.3 mW. The loops on left column were obtained after the SL was thermally erased in the presence of a negative external field, $H < 0$. The loops in the right column were similarly erased, but under a positive field, $H > 0$.

that of SL. Therefore, the RL loop traces lack any indication of the coupling strength between the two magnetic layers. The decreasing Kerr angle with the magnetic field after magnetization reversal and the deviation of the loop from squareness are consequences of competition among exchange coupling from SL, exchange coupling within RL, the applied magnetic field, and the nonuniform temperature distribution within the RL.

In Fig. 4, the loop at $P_0 = 0.7$ mW is tilted, indicating that the RL magnetization at this power is not perpendicular to the plane of the film. When P_0 is increased to 1 mW, the RL magnetization in the hot region becomes perpendicular, and the Kerr loop becomes square. (Since the light is focused on the film through the glass substrate, the Faraday effect in the glass substrate gives rise to the slope seen at the top and bottom of the loops). As P_0 exceeds 1 mW, the shift of the loops becomes obvious: the loops in the left column shift to the positive field side, while those in the right column shift in the opposite direction.

Ideally, if the SL magnetization is uniform, its stray field will be zero outside the SL, and there will be no magneto-static coupling between RL and SL. But, because of the non-uniform temperature distribution in the focused spot, locally nonuniform SL magnetization gives rise to a nonzero magneto-static field in the RL. Since the SL compensation temperature is around room temperature, the stray field from SL favors a parallel RL magnetization with the SL magnetization. This causes the loops in the left column of Fig. 4 to be shifted to the right, while those in the right column to be shifted to the left. From these loops, the strength of magneto-static coupling between RL and SL is seen to be less than 50 Oe.

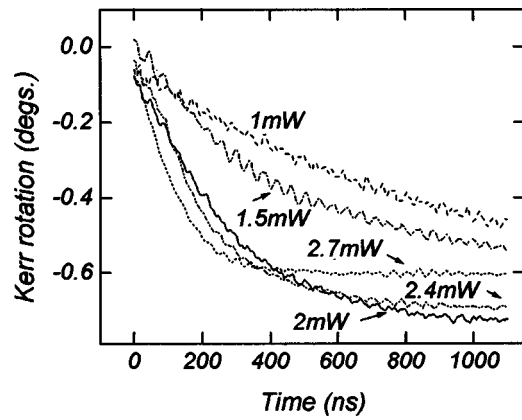


FIG. 5. Kerr rotation signal from the read layer vs time for sample 1 during irradiation with a $1.1 \mu\text{s}$ laser pulse. Different curves correspond to different laser powers; in all cases the pulse starts at $t = 0$.

Comparing Figs. 3 and 4, it is evident that H_b has opposite polarity between sample 1 and 2. Strong exchange coupling in sample 1 tilts the Kerr loops. Also, there is no sharp transition from in-plane to perpendicular magnetization with the read power in sample 1.

B. Transient thermal response of the Kerr signal

To observe the dynamic process of copying domains from SL to RL, we monitored the transient variation of the RL Kerr signal during irradiation after a laser pulse and the results are shown in Figs. 5 and 6. In these figures, different curves correspond to different laser powers. The experimental procedure for obtaining Figs. 5 and 6 is as follows: (1) saturating the SL magnetization under $H < 0$; (2) switching on a laser pulse at $t = 0$ and recording the differential MO and sum signals simultaneously; (3) saturating the SL magnetization under $H > 0$; (4) repeating step (2) above. Normalize the differential signals from steps (2) and (4) by the sum signals and subtract them from each other, then the transient variations of θ_k are therefore obtained.

For sample 1, the exchange coupling between RL and SL prefers a parallel alignment of the magnetic moments of transition metals in the RL with those in the SL causing $\theta_k \leq 0$, as shown in Fig. 5. For sample 2, since the stray field in

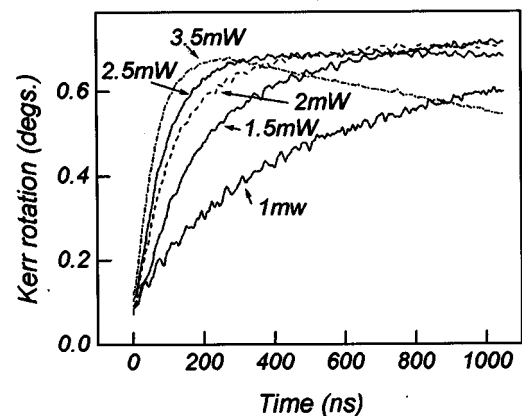


FIG. 6. Same as Fig. 5 but for sample 2.

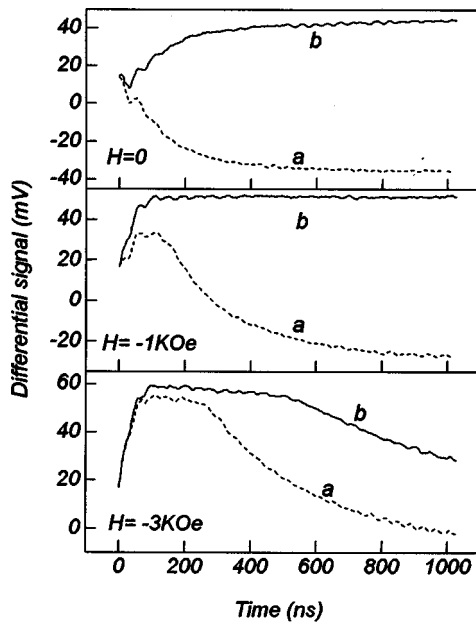


FIG. 7. Variation of the differential signal vs time at $H=0$, -1 , and -3 kOe for sample 1. Curves (a) were obtained with the SL initially saturated with a negative applied field, $H<0$. Similarly, curves (b) correspond to initial saturation of the SL with a positive field, $H>0$. In all cases, the laser power incident on the film was 2 mW.

RL favors a parallel alignment of magnetization of RL with that of SL and the RL magnetization is dominated by G_d , θ_k is larger than zero, as displayed in Fig. 6.

In Figs. 5 and 6, θ_k increases with time. At $t \approx 0$, the RL magnetization lies within the film plane, and therefore, the polar Kerr effect is negligible. As the laser pulse causes the temperature in the area of the focused spot to rise; the RL magnetization becomes perpendicular and θ_k increases rapidly. At low laser power, for example, 1 and 1.5 mW on sample 1 and 1 mW on sample 2, θ_k increases with time even though the temperature in the films is substantially stabilized after a few hundred nanoseconds. At medium laser power, e.g., 2–2.4 mW on sample 1 and 1.5–2.5 mW on sample 2, θ_k reaches its maximum and remains saturated afterwards. At high laser power, the maximum θ_k value of sample 1 is reduced (see the curve corresponding to $P_0 = 2.7$ mW in Fig. 5); but for sample 2, the θ_k value first reaches its maximum, then it decreases (see the curve corresponding to $P_0 = 3.5$ mW in Fig. 6). The reduction of θ_k at 3.5 mW for sample 2 may be ascribed to the formation of a reverse domain in the SL. For sample 1, at high laser power, the aperture in which RL has perpendicular magnetization is large, but θ_k decreases with temperature, resulting in the reduction of the measured Kerr signal.

From Figs. 5 and 6, it is evident that a very small coupling field is sufficient to insure the copying from SL to RL; there is no abrupt change in the monitored Kerr signals. The transient behavior of the Kerr signal comes mainly from the thermal response of the magnetic films under the focused beam, which depends to a large extent on the multilayer stack of the samples.

To explore the effect of magnetic coupling between the RL and SL on the dynamic processes underlying the Kerr

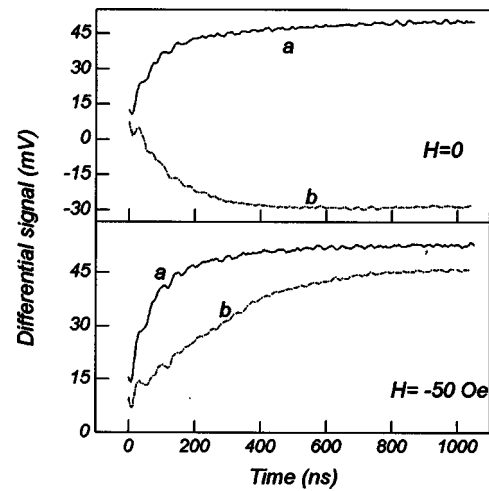


FIG. 8. Variations of differential signals vs time at $H=0$ and -50 Oe for sample 2. Curves (a) were obtained with the SL initially saturated with a negative applied field, $H<0$. Similarly, curves (b) correspond to initial saturation of the SL with a positive field, $H>0$. In all cases, the laser power incident on the film was 2 mW.

signal, a magnetic field was applied during the laser pulse. Figures 7 and 8 show the differential MO signal ΔS versus time at various applied magnetic fields. Curves (a) and (b) in Figs. 7 and 8 were obtained when SL was initially saturated with $H<0$ and $H>0$, respectively. The variation of ΔS with time depends on temperature, magnetic coupling between RL and SL, and the strength of the external field.

In curve b of Fig. 7, the exchange coupling between RL and SL favors the RL magnetization parallel to the external field; ΔS then saturates earlier at higher magnetic field. (At $H = -3$ kOe, the reduction of ΔS in curve (b) at $t > 500$ ns is because of the formation of a reverse domain in the hot region). In curves (a) of Fig. 7, the external field is anti-parallel to the exchange field between RL and SL; the relative strengths between the exchange field and the external field determine the orientation of the RL magnetization. At $H = -1$ and -3 kOe, the RL magnetization first follows the external field, resulting in $\Delta S > 0$; it then deviates from the external field, and finally follows the exchange field, as evidenced by $\Delta S < 0$ in curves (a) of Fig. 7. This confirms the increase of the exchange field with temperature. At the time when curve a begins to deviate from curve (b), the exchange field is approximately equal to the external field.

For sample 2, the situation is substantially different. In the case of curves (b) in Fig. 8, the stray field from SL is anti-parallel to the external field. Since the stray field in the RL film is weak, a 50 Oe field can overcome the stray field, as evidenced by the changes in curves (b) of Fig. 8. At $H = -50$ Oe, the RL magnetization does not follow that of SL but follows the external field.

From Figs. 7 and 8, we deduce that the transient behavior of the Kerr signal depends not only on the thermal characteristics of the films but also on the magnetic coupling between RL and SL.

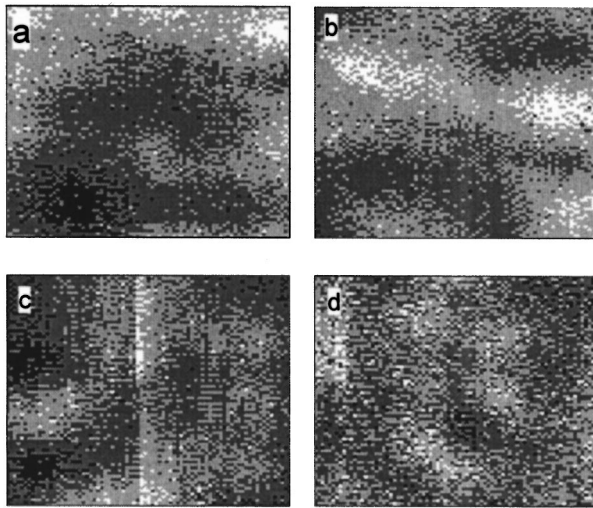


FIG. 9. Gray-level images of the disk surface. (a), (b), and (c) are on sample 1, and (d) is on a conventional MO disk. Frames (a) and (d) were obtained at $H=0$, while frames (b) and (c) were obtained at $H=100$ and -100 Oe, respectively. Dimensions of each frame are $5.4 \times 4.2 \mu\text{m}$. The gray scale for frames (a), (b), and (c) is from 45 mV (black) to 54 mV (white), and that for frame (d) is from 51 mV (black) to 54 mV (white). In all cases, the laser power incident on the sample is 1 mW.

C. Random orientations of the RL magnetization

Figure 9 displays gray-level images of sample 1 when a small area of the film was scanned. These images were obtained by scanning the film while monitoring the differential signal ΔS . Prior to scanning, the area of the sample was thermally erased at $H > 0$. During scanning, an external field may be applied. For comparison, an image for a conventional MO disk (d), is also displayed. The contrast seen in these images gives rise to media noise in readout. From (a), it is seen that the variations of ΔS over the scanned region, from 45 to 54 mV, are quite small. Also, these variations of ΔS

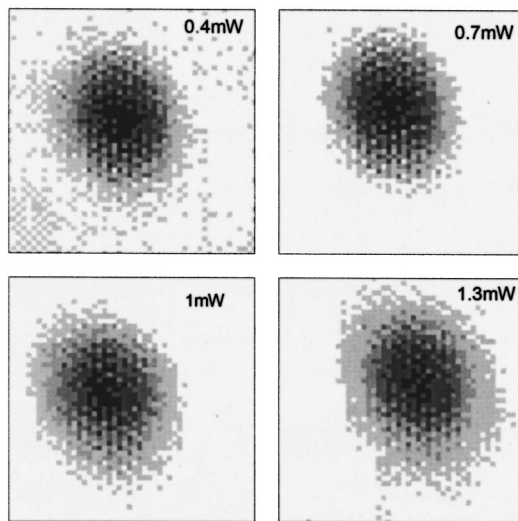


FIG. 10. Scanning micrographs of a magnetic domain in the SL of sample 1. During each scan, the Kerr angle is monitored. Frames (a) to (d) correspond to read laser powers of 0.4, 0.7, 1, and 1.3 mW, respectively. No magnetic field was applied during scanning. Dimensions of each frame are $5 \times 5 \mu\text{m}$, and the gray scale for all frames is from -0.78° (black) to 1° (white).

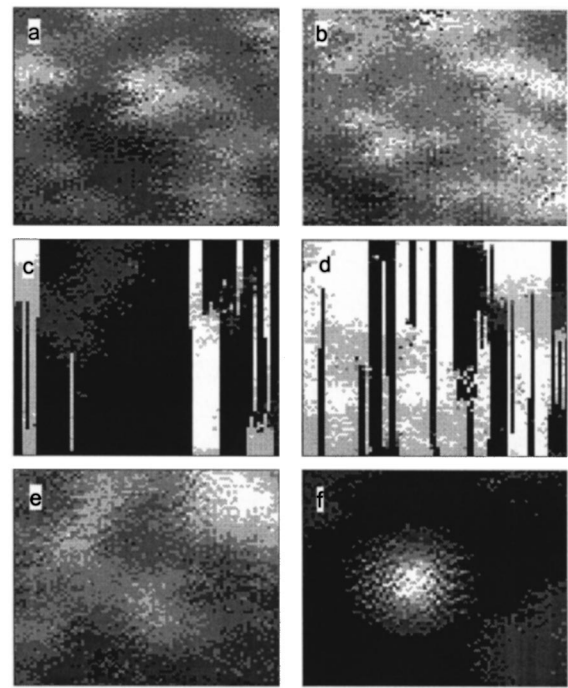


FIG. 11. Gray-level images of the surface of sample 2, obtained by scanning a small area while monitoring the differential signal. Dimensions of each frame are $5.4 \times 4.4 \mu\text{m}$ and the power of the laser beam is 1.3 mW during scanning. Prior to scanning, the SL was thermomagnetically erased with a positive applied field, $H > 0$. Frames (a)–(f) were obtained at $H=0, 75, -25, -25, -35,$ and 0 Oe, respectively. (c) and (d) correspond to different regions of the sample. The gray scale in (a) is from -21 mV (white) to -34 mV (black); in (b) it is from -29 mV (white) to -38 mV (black); in (c) it is from 60 mV (white) to -35 mV (black); in (d) it is from 50 mV (white) to -30 mV (black); in (e) it is from 34 mV (white) to 50 mV (black); and in (f) it is from 50 mV (white) to -35 mV (black).

seem to be insensitive to ± 100 Oe applied field [see frames (b) and (c)]; strong exchange coupling keeps the RL magnetization in order. For the conventional MO disk, the variations of ΔS over the scanned region are from 51 to 54 mV, which is less than those for sample 1. Lower readout noise, therefore, might be expected in the conventional MO disk than in sample 1.

Figure 10 shows gray-level images of reading a large domain on sample 1 at $P_0=0.4, 0.7, 1,$ and 1.3 mW. It is evident that the images at $P_0=0.7$ and 1 mW have the best contrast. At $P_0=0.4$ mW, besides the domain, gray dots are visible everywhere in the frame, probably due to inhomogeneity. At low reading power, the temperature in the hot spot is close to in-plane-to-perpendicular magnetization transition temperature, and inhomogeneity will cause large fluctuations of polar Kerr rotation. In Fig. 10, it is also seen that, due to the finite size of focused spot, the domain has a wide boundaries having different contrast from its center.

Figure 11 shows gray-level images for sample 2, obtained under various magnetic fields. Note that each frame in Fig. 11 has a different scale of gray. The variations of ΔS exhibited in frame (a) of Fig. 11 are larger than those in Fig. 9. More media noise is therefore expected for sample 2 than for sample 1, as well as for the conventional MO disk. When a 75 Oe external field is applied, ΔS over the scanned area becomes more uniform, as evidenced from frame (b) of Fig.

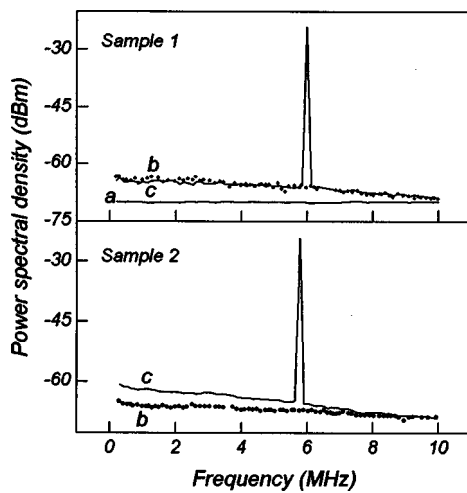


FIG. 12. Noise spectra at the differential output of a MO readout system for samples 1 and 2. Trace (a), obtained with light blocked from reaching the detectors, is the thermal noise level; trace (b), obtained with the disk spinning while the focused laser beam reading an erased track, is the erased noise levels; and trace (c), obtained with the disk spinning while the focused laser beam reading a written track, is carrier plus total noise levels. The read laser power is 3.2 mW on sample 1 and 2.3 mW on sample 2. The reflected optical power from both samples is the same, however, being $21.5 \mu\text{W}$ on each detector. The velocity of the track under the focused spot is 9.4 m/s in both cases.

11. This means that the orientation of the RL magnetization in sample 2 has some random behavior at $H=0$.

If there is no coupling between RL and SL, the RL magnetization will be random when it switches from in-plane to perpendicular direction in the hot region of the focused spot. In frames (c) and (d) of Fig. 11, about -25 Oe field is applied for fully or partially cutting off the magneto-static coupling between RL and SL. Many black stripes, which have the same magnetization orientation as in frame (a), are visible on the white background. (The magnetization in the white area is reversed from that in the black stripes.). The orientation of magnetization at $H = -25 \text{ Oe}$ seems random. Moreover, the stripes are usually parallel to the direction of scanning. (In the experiment, the film was scanned along the vertical direction after each step jump in the horizontal direction).

The observed behavior in frames (c) and (d) of Fig. 11 can be explained as follows. In some pixels, the RL magnetization prefers to be "black." At the next pixel during scanning, the magnetization can "see" the magnetization of the preceding pixel through thermal cross talk. To achieve minimum energy, the RL magnetization of this region will be aligned parallel to that of the previous region. In this way, the focused spot drags the black magnetization pixels consecutively until it reaches a site where the magnetization prefers to be "white." This random Kerr signal gives rise to very high noise levels.

In frame (e) of Fig. 11, the external field is larger than the coercivity plus the magneto-static coupling field; the RL magnetization is reversed from that of frame (a). Once again, the nonuniformity of the Kerr signal is observed. In frame (f), a domain is written in the SL, and the scanning micrograph shows the domain as copied onto the RL.

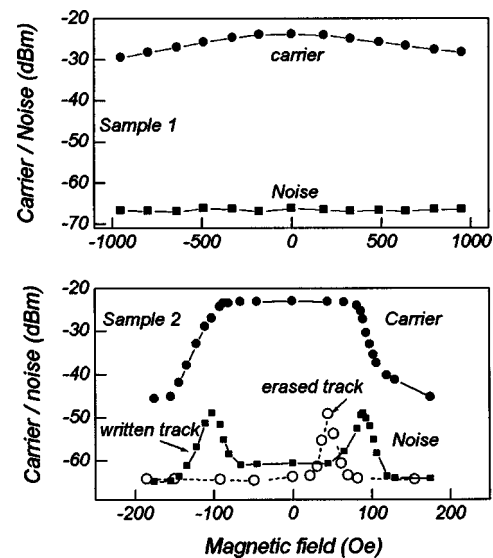


FIG. 13. Measured carrier level and noise density as functions of the applied magnetic field for samples 1 and 2. On recorded tracks, carrier and noise levels are obtained at 5.77 MHz. (5.77 MHz is the tone frequency of the recorded marks.). For sample 2, noise levels on the erased track were measured at 3 MHz.

D. Signal and noise

The recording and readout behavior of the two disks were examined using a dynamic tester. At a mark length of $0.45 \mu\text{m}$, CNR was about 40.5 dB for sample 1 and 35.8 dB for sample 2. Figure 12 shows the power spectral density at the differential output of a MO readout system for the two samples. Curve (a) is thermal noise levels. Curves (b) and (c) are total noise, obtained while reading an erased and a recorded track, respectively. For sample 1, the noise density obtained from a written track is almost the same as that from an erased track. For sample 2, however, the noise floor of a recorded track is a few dB higher than that of an erased track.

To look into the effect of magnetic coupling on signal and noise, an external magnetic field was applied during readout. Figure 13 shows that the carrier and noise levels as functions of the magnetic field. In this figure, $H > 0$ means that the magnetic field is parallel to the bias field for writing; and $H < 0$ means that the field is anti-parallel to the bias field. For sample 1, the carrier level is seen to decrease gradually with H , but the noise level does not change. For sample 2, the carrier level does not change until $|H| > 80 \text{ Oe}$, and the noise level has abnormal peaks at certain magnetic fields. On the recorded track, there are two noise peaks, one at $H \approx 90 \text{ Oe}$ and the other at $H \approx -100 \text{ Oe}$; on the erased track, only one noise peak appears, and the field at this peak is much lower than that of the recorded track.

Figure 14 shows the noise density on the ungrooved regions for sample 2. The same noise phenomena are seen to exist on the ungrooved regions of the sample, but the fields at the noise peaks are different from those on the grooved track. Also, the peak noise levels on the ungrooved region are much lower than those on the grooved one (compare Fig. 14 with Fig. 13 for sample 2). On the erased ungrooved region, the field at the noise peak is about 25 Oe, which is

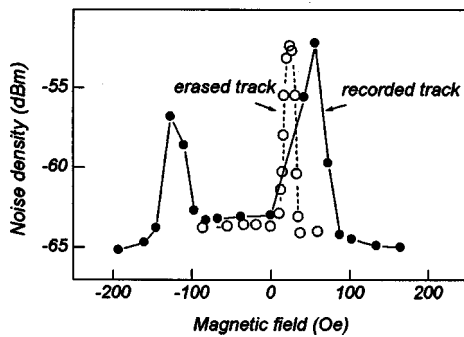


FIG. 14. Measured noise density on an ungrooved region of sample 2 at 2 MHz, plotted vs the applied magnetic field. The read laser power is 2.6 mW, and the track velocity under the focused spot is 11.6 m/s.

the same as the field applied to obtain frames (c) and (d) of Fig. 11. On the recorded region, the fields at the two noise peaks are about 60 and -120 Oe, respectively. The higher peak noise levels on the grooved region probably reflect the magnetization randomness induced by the roughness of the groove profiles.

The observed behavior of carrier and noise for the samples can be understood from the magnetic coupling between RL and SL. For sample 1, RL and SL are strongly exchange-coupled and the RL magnetization follows that of SL. If the external field is less than the SL coercivity plus the exchange field, the noise levels will not change with H , but the carrier levels decrease gradually with increase of H because H pulls the RL magnetization toward it, increasing the observed domain size.

For sample 2, when the effective field (external field plus stray field from SL) is nearly zero, the RL magnetic moments will be randomly oriented, as demonstrated in frames (c) and (d) of Fig. 11. On the erased track, the stray field in RL (from SL) is parallel to the direction of the bias field for erasure; so an appropriate positive field can nullify the effect of stray field, leading to very high noise levels. On the recorded track, the stray field in RL can take a positive or negative value, depending on the SL magnetization state. So, either a negative or a positive field of proper magnitude can randomize the RL magnetization. Moreover, since the stray field produced by the recorded SL is higher than that by the erased SL, the external fields required to have maximum random noise are higher on the recorded track than on the erased one (see Figs. 13 and 14).

In practice, the data marks recorded on a CAD-MSR disk are read at $H=0$; therefore, the peak noise displayed in Figs. 13 and 14 might not appear, but noise caused by the random orientation of RL magnetization still exists. For sample 2, the stray field is not uniform on the recorded region, and, in particular, it goes to zero at the domain boundaries.¹³ The orientations of the RL magnetic moments in these areas will become more or less random, giving rise to noise. This explains why, for sample 2, the noise levels on a recorded track are higher than those on an erased track (see Figs. 12 and 13 for sample 2). Moreover, in some cases, a magnetic layer such as GdFe alloy is inserted between RL and SL to suppress the effect of SL on RL by reducing the

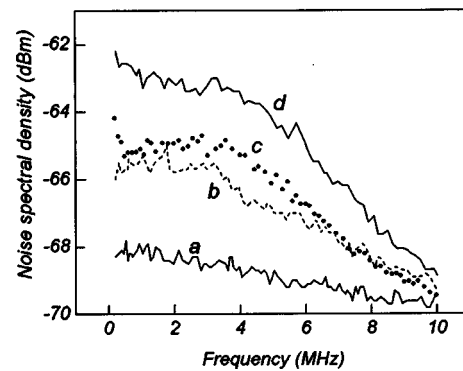


FIG. 15. Noise spectra obtained from an ungrooved region of (a) a conventional MO disk, (b) sample 1, and (c) and (d) sample 2. Curves (a)–(c) were obtained on erased tracks, while curve (d) was obtained from a recorded track. (Carrier removed from the curve for clarity.) In all cases, the track velocity under the focused spot is 11.6 m/s, and the reflected optical power reaching each detector is $21.5 \mu\text{W}$.

exchange coupling between these layers.⁶ The stray field formed by the SL magnetization and intermediate layer may thus cancel the exchange coupling, causing a random magnetization within the RL.

To directly compare the noise levels among sample 1, sample 2, and a conventional MO disk, we show in Fig. 15 traces of the noise levels on the ungrooved region for both samples, as well as for a conventional MO disk. On an erased ungrooved region, the conventional MO disk has the lowest noise levels, and that sample 1 has almost the same noise levels as sample 2. On the recorded region, sample 2 has a higher noise floor than sample 1. These results are in agreement with those exhibited in Figs. 9 and 11.

IV. CONCLUSIONS

We have investigated the magnetic coupling between two magnetic layers, transient thermal response, and carrier and noise for two CAD-MSR samples. For the exchange-coupled disk, it appears that the strength of the coupling increases with temperature. The Kerr loop of the readout layer does not have a square shape. For the magneto-statically coupled disk, the coupling, usually weak, depends on the nonuniformity of magnetization in the storage layer. The readout layer has a square Kerr loop. The perpendicular magnetization in the hot region of the focused spot is randomly oriented if the stray field from the storage layer is close to zero. This causes a high readout noise levels when the track is recorded. So the strength and mode of coupling between the two magnetic layers seems to be critical for CAD-MSR media to exhibit high signal and low noise levels.

¹K. Aratani, A. Fukumoto, M. Ohta, M. Kaneko, and K. Watanabe, Proc. SPIE **1499**, 209 (1991).

²K. Tamanoi and K. Shono, J. Magn. Soc. Jpn. **19**, 421 (1995).

³Y. Murakami, N. Iketani, J. Nakajima, A. Takahashi, K. Ohta, and T. Ishikawa, J. Magn. Soc. Jpn. **17**, 201 (1993).

⁴K. Matsumoto and K. Shono, J. Magn. Soc. Jpn. **19**, 335 (1995).

⁵Y. Murakami, A. Takahashi, and S. Terashima, IEEE Trans. Magn. **31**, 3215 (1995).

- ⁶N. Nishimura, T. Hiroki, T. Okada, and S. Tsunashima, *J. Appl. Phys.* **79**, 5683 (1996).
- ⁷Y. Suzuki, K. Tanase, A. Yamaguchi, S. Murata, S. Sumi, and K. Torazawa, *IEEE Trans. Magn.* **32**, 4067 (1996).
- ⁸J. Hirokane and A. Takahashi, *Jpn. J. Appl. Phys., Part 1* **35**, 5701 (1996).
- ⁹K. Torazawa, S. Sum, S. Yonezawa, N. Suzuki, Y. Tanaka, A. Takahashi, Y. Murakami, and N. Ohta, *IEICE Trans. Electron.* **E80-C**, 1142 (1997).
- ¹⁰A. Takahashi, Y. Murakami, J. Hirokane, J. Nakayama, Y. Kurata, and H. Yamaoka, *Jpn. J. Appl. Phys., Part 1* **36**, 500 (1997).
- ¹¹T. Kawano and H. Ito, US Patent No. 5,621,706 (1997).
- ¹²M. Mansuripur *et al.*, *Appl. Opt.* **36**, 9296 (1997).
- ¹³M. Kaneko and A. Nakaoki, *J. Magn. Soc. Jpn.* **20**, 7 (1996).